Numerical study of the effects of pressure and gravitational acceleration on soot formation in laminar axisymmetric coflow methane/air diffusion flame

Liu, Fengshan; Smallwood, Gregory J.; Kong, Wenjun

Publisher's version / Version de l'éditeur:

Proceedings of the 2009 ASME Summer Heat Transfer Conference, 2009-07

Proceedings of HT2009
2009 ASME Summer Heat Transfer Conference
July 19-23, 2009, San Francisco, California USA

HT2009-88259

NUMERICAL STUDY OF THE EFFECTS OF PRESSURE AND GRAVITATIONAL ACCELERATION ON SOOT FORMATION IN LAMINAR AXISYMMETRIC COFLOW METHANE/AIR DIFFUSION FLAME

Fengshan Liu
ICPET, National Research Council
Ottawa, Ontario, Canada

Gregory J. Smallwood
ICPET, National Research Council
Ottawa, Ontario, Canada

Wenjun Kong
Institute of Engineering Thermophysics
Chinese Academy of Sciences
Beijing, China

ABSTRACT

The structure and soot formation characteristics of a coflow laminar methane/air diffusion flame under conditions of constant p^2g and mass flow rates of the air and fuel streams were numerically investigated in order to examine the validity of the p^2g scaling relationship. The p^2g scaling relationship has been used to experimentally investigate soot formation in weakly-buoyant laminar diffusion flames by conducting experiments at reduced pressures. Detailed numerical calculations were conducted by solving the elliptic conservation equations of mass, momentum, species, and energy in axisymmetric cylindrical coordinates using a standard control volume method. Detailed multi-component thermal and transport properties and detail combustion chemistry were employed in the modelling. Soot formation was modeled using a semi-empirical acetylene based model in which two transport equations for the soot mass fraction and soot number density per unit mass were solved. Thermal radiation was calculated using the discrete-ordinates method and a 9-band non-grey model for the radiative properties of the CO-CO_2-H_2O-soot mixture. The flame structure and soot formation characteristics exhibit strong dependence on the ambient pressure even though p^2g and the mass flow rates are kept constant. Significantly more soot is produced with increasing the pressure and decreasing the gravity level. Numerical results clearly demonstrate that the p^2g scaling relationship is invalid as far as soot formation is concerned.

INTRODUCTION

Investigation of soot formation is of great importance both fundamentally and practically. Although laminar coflow diffusion flames at atmospheric pressure and normal gravity (ng) are an ideal flame configuration to study many fundamental physical and chemical aspects of soot formation experimentally and numerically, such flames are in general buoyancy controlled. On the other hand, practically important turbulent flames are often not buoyancy controlled and should be related to weakly-buoyant laminar diffusion flames. Because of these constraints, it has been argued that the findings gained in buoyant laminar flames at ng may not be relevant to turbulent flames, since the path that soot follows has very different temperature and chemical environments in buoyant and weakly-buoyant flames, leading to very different soot growth and oxidation history [1,2].

Weakly- or non-buoyant laminar diffusion flames are ideally studied in environment of reduced gravity. Two popular but expensive ways to create such environment are using a space shuttle or a drop tower. Another inexpensive and easy-to-achieve approach to study laminar diffusion flames under reduced gravity is to investigate laminar diffusion flames under reduced pressure and normal gravity based on the simple scaling relationship that buoyancy scales as p^2g in laminar flames [3,4]. This scaling relationship suggests that flames at pressures on the order of 0.l atm and normal gravity (1g) have the same structure as those at reduced gravity of the order of 0.01g and atmospheric pressure. Based on this principle, Faeth and co-workers have experimentally investigated soot properties in weakly-buoyant laminar diffusion flames at low

pressures and normal gravity [1,5]. It is important to point out that this simple scaling relationship was derived by maintaining the constancy of the following nondimensional parameters: the Reynolds number, the Peclet number, and the Richardson number [3]. The derivation relies on the assumptions of a flame sheet model, unity Lewis number, and neglect of radiation heat loss [3]. However, there is currently a lack of detailed experimental or numerical studies as to whether such a scaling can be applied to investigate soot properties, even though applications have been reported [1,5].

The present study made an attempt to address the following question: does a laminar diffusion flame at lower pressure and higher gravitational acceleration have the same flame structure and soot field as its counterpart at a higher pressure and lower gravity as long as p^2g and the mass flow rates of fuel and air are kept constant? To answer this question, detailed numerical calculations were conducted to predict the flame properties of laminar axisymmetric coflow methane/air diffusion flame under different pressures and gravities while keeping the mass flow rates of fuel and air and p^2g constant. Governing equations of mass, momentum, energy and species were solved in axisymmetric cylindrical coordinates using the standard finite volume method. Soot formation was modelled using a semi-empirical two-equation model. Thermal radiation transfer was accounted for using the discrete-ordinates method coupled with a wide-band non-grey property model. Combustion chemistry was modelled using the GRI-Mech 3.0 mechanism. Detailed thermal and transport properties were considered. The numerical results were presented and analyzed with attention paid to the validity of the p^2g scaling relationship for flame properties and in particular those related to soot.

NUMERICAL MODEL AND SOLUTION METHOD

The elliptic steady-state governing equations of mass, momentum, energy, and species in axisymmetric cylindrical coordinates and in the low Mach number limit given in [6] were solved. The effect of buoyancy was accounted for by retaining the gravity term in the momentum equation in the flow direction (z, vertically upwards). The method of correction diffusion velocity described in [7] was employed to ensure that the net diffusion flux of all species sums to zero in both r and z directions. Note that the correction velocity accounts for the thermophoretic velocity of soot. The interaction between the soot chemistry and the gas-phase chemistry was accounted for through the reaction rates of the species related to soot formation and oxidation, namely C_2H_2, CO, H_2, O_2, O, H, and OH in the present context. Only the thermal diffusion velocities of H_2 and H are accounted for using the expression given in [7]. The source term in the energy equation due to radiation heat transfer was also included.

A modified version of the semi-empirical two-equation formulation of soot kinetics proposed by Leung et al. [8] was used to model soot nucleation, growth and oxidation. The transport equations for the soot mass fraction and number density are given as

$$\rho u\frac{\partial Y_s}{\partial z}+\rho v\frac{\partial Y_s}{\partial r}=-\frac{\partial}{\partial z}\left(\rho V_{T,z}Y_s\right)-\frac{1}{r}\frac{\partial}{\partial r}\left(r\rho V_{T,r}Y_s\right)+S_m \quad (1)$$

$$\rho u\frac{\partial N}{\partial z}+\rho v\frac{\partial N}{\partial r}=-\frac{\partial}{\partial z}\left(\rho V_{T,z}N\right)-\frac{1}{r}\frac{\partial}{\partial r}\left(r\rho V_{T,r}N\right)+S_N \quad (2)$$

where u and v are velocities in the streamwise (z) and radial (r) directions, ρ is the mixture density, Y_s is the soot mass fraction and N is the soot number density defined as the particle number per unit mass of mixture. Quantities $V_{T,r}$ and $V_{T,z}$ are the thermophoretic velocities of soot in r and z directions, respectively, and are calculated as [9]

$$V_{T,x}=-0.65\frac{\mu}{\rho T}\frac{\partial T}{\partial x} \quad x=r,z \quad (3)$$

The source term S_m in Eq.(1) accounts for the contributions of soot nucleation, surface growth and oxidation. In this simplified soot nucleation and growth model, it is assumed that acetylene is the only soot nucleation and growth species and soot nucleation and surface growth proceed respectively via $C_2H_2 \rightarrow 2C(S) + H_2$ and $C_2H_2 + nC(S) \rightarrow (n+2)C(S) + H_2$. The rates of nucleation and surface growth are given as $R_1=k_1(T)[C_2H_2]$ (kmol/m^3/s) and $R_2=k_2(T)A_s^{0.5}[C_2H_2]$ (kmol/m^3/s), where $A_s=\pi(6/\pi)^{2/3}\rho_{C(S)}^{-2/3}\ Y_s^{2/3}\ \rho N^{1/3}$ is the soot surface area per unit volume and $[C_2H_2]$ is the mole concentration of acetylene. The nucleation and growth rate constants used in the present calculations were taken from our previous study [9]: k_1 = 1000exp(–16103/T) [1/s] and k_2 = 1750exp(–10064/T) [m$^{0.5}$/s]. The density of soot $\rho_{C(S)}$ is taken to be 1.9 g/cm^3. It is noted that the soot surface growth rate is assumed here to be proportional to the square root of the soot surface area based on the recommendation of Leung et al. [8]. Possible physical reasons behind this sub-linear dependence of the surface growth rate on soot surface are particle aggregation and reduction in soot surface reactivity.

The source term in the soot mass fraction equation can be written as

$$S_m=2M_{C(S)}(R_1+R_2)-(2R_3+R_4+R_5)A_s \quad (4)$$

where $M_{C(S)}$ is the molar weight of soot (assumed to be the same as carbon), R_3, R_4, and R_5 are the specific soot oxidation rates by O_2, OH, and O, respectively. Soot oxidation was assumed to proceed through the following reactions

$O_2 + 0.5C(S) \rightarrow CO$, $OH + C(S) \rightarrow CO + H$, $O + C(S) \rightarrow CO$

The reaction rates per unit surface area of these three reactions (kg m^{-2} s^{-1}) are given as

$$R_3=120\left\{\frac{k_A X_{O_2}P_a\chi}{1+k_Z X_{O_2}P_a}+k_B X_{O_2}P_a(1-\chi)\right\},\ \chi=\left\{1+\frac{k_T}{k_B X_{O_2}P_a}\right\}^{-1} \quad (5)$$

$$R_4=\varphi_{OH}k_4(T)T^{-1/2}X_{OH}P_a \quad (6)$$

$$R_5=\varphi_O k_5(T)T^{-1/2}X_O P_a \quad (7)$$

where X_{OH} and X_O denote the mole fractions of OH and O, P_a is the ambient pressure in atm, and φ_{OH} and φ_O are the collision efficiencies for OH and O attack on soot particles. The rate of soot oxidation by O_2 was based on the Nagle-Strickland-Constable model [10] with rate constants for R_3 and R_4 taken from [11]. A constant collision efficiency of 0.2 was assumed

for both OH and O. The rate constants for R_5 were taken from [12].

The source term S_N in Eq.(2) represents the production of the number density of soot particles due to nucleation

$$S_N = \frac{2}{C_{min}} N_A R_1 \quad (8)$$

where N_A is Avogadro's constant (6.022×10^{26} kmol^{-1}) and C_{min} is the number of carbon atoms in the incipient soot particle (700, which gives a soot incipient particle diameter of about 2.4 nm). It is noted that the destruction of number density by agglomeration is neglected for the reasons discussed in [9]. The density of the mixture (including soot) was calculated using the ideal gas state equation

$$\rho = \frac{P_a}{R_u T \sum_{k=1}^{KK} Y_k / W_k} \quad (9)$$

where R_u is the universal gas constant and KK the number of gas-phase species.

The source term due to thermal radiation in the energy equation was calculated using the discrete-ordinates method in axisymmetric cylindrical geometry described in [13]. The statistical narrow-band correlated-K (SNBCK) based 9-band model developed by Liu and Smallwood [14] was employed to obtain the absorption coefficients of the combustion products containing CO, CO_2, H_2O, and soot at each band and each quadrature point.

Gas-phase combustion chemistry was modeled using the GRI-Mech 3.0 mechanism [15], which was optimized for methane combustion, with the removal of species and reactions related to NO_x formation (except N_2). This simplified GRI-Mech 3.0 mechanism contains 36 species and 219 reactions. Thermal and transport properties of species and the mixture were obtained from CHEMKIN subroutines and the GRI-Mech 3.0 database.

To identify the location of the flame sheet defined by the stoichiometric mixture fraction, an additional transport equation for the mixture fraction (0 at the air streams and 1 at the fuel stream), which is a conserved quantity without source terms in its transport equation, was solved. The diffusion coefficient of the mixture fraction was calculated with the assumption of unity Lewis number after the study of Pitsch and Peters [16]. In addition, the mixture fraction definition given by Bilger et al. [17] was also used to identify the flame location.

The transport equations for mass, momentum, energy, gas-phase species, soot mass fraction, soot number density, and radiation intensity are closed with the equation of state and appropriate boundary conditions on each side of the computational domain. These equations were discretized using the control volume method [18]. Diffusion and convective terms in the conservation equations are discretized respectively using the central and upwind difference scheme. The SIMPLE numerical algorithm [18] was used to treat the pressure and velocity coupling. Governing equations of momentum, energy, soot mass fraction and number density were solved using the tridiagonal-matrix algorithm (TDMA). Governing equations of the gas-phase species were solved in a fully coupled fashion at every computational control volume using a direct solver to speed up the convergence process [19].

The axisymmetric coflow laminar CH_4/air diffusion flames numerically investigated in this study are stabilized on a burner similar to the Gülder burner described in [20], which is also very similar to the burner used by Santoro and co-workers [21,22]. The Gülder burner consists of a fuel tube of 10.95 mm inner diameter surrounded by a co-annular outer air jet of 100 mm inner diameter. The thickness of the fuel tube is 0.9 mm. In this numerical study, the burner is a modified version of the Gülder burner: the outer co-annular air jet is much larger and has an inner diameter of almost 28 cm. This serves the purpose of minimizing the influence of using slip boundary condition on the outer radial boundary on the flame structure.

Numerical calculations were conducted on a computational domain of 9.78 cm (z) × 13.98 cm (r). Non-uniform grids were used in both the r and z directions to provide greater resolution in regions of high gradients near the burner exit without an excessive increase in the computing time. Very fine and uniform grids were placed within the fuel pipe at r = 5.45 mm in the radial direction with a grid size less than 0.2 mm. Outside the burner tip in r direction, the grid size became gradually coarser. In the flow direction (z), very fine and non-uniform grids were used in the burner exit region up to 2.6 cm (grid size less than 0.36 mm). Further downstream, uniform but coarser grids were used. The grid size between z = 2.6 cm and 6.6 cm is still fairly fine at Δz = 0.4 mm. Beyond z = 6.6 cm, the grid size is Δz = 0.65 mm. The computational domain was divided into 251(z)×135(r) control volumes. Both the fuel and air inlet temperatures were assumed to be 300 K. A uniform velocity profile was assigned to the air inlet except near the outer surface of the fuel pipe where a boundary layer type velocity profile was assumed. For the fuel stream, the inlet velocity profile was assumed to be parabolic. Along the centerline (r = 0 cm) and the outer radial boundary (r = 13.98 cm), v = 0 cm/s and zero-gradient for all other variables are assumed. At the top boundary (z = 9.78 cm), a zero-gradient condition was applied to all variables. The convergence criterion used in the calculations was that relative changes of the peak soot volume fraction and the peak temperature were to be less than 1×10^{-5}. The grid resolution was found adequate, since further refinement has negligible influence on the numerical results.

This numerical approach (with the simple soot formation model) has been shown to predict soot volume fraction and flame temperature distributions in fairly good agreement with experimental data at atmospheric and elevated pressures [13,23]. It is believed that the flame model described above is adequate to investigate the validity of the p^2g scaling relationship, since both the pressure and the gravitational acceleration affect soot formation mainly physically rather than chemically.

RESULTS AND DISCUSSION

Numerical calculations were conducted under five different levels of pressure and gravity at a constant p^2g = 490 atm^2 cm/s^2. The five sets of pressure and gravity are summarized in Table 1, where g_0 is the gravity on earth (980 cm/s^2). It is seen that while the pressure does not vary significantly from the lowest to the highest level (by a factor of 4). However, the corresponding variation of gravitational acceleration is much larger (a factor of 16). It is recognized that the range of pressure variation considered in this study is relatively small. This is to ensure that the methodology used in this numerical study, in particular the gas-phase reaction mechanism, soot formation model, and the neglect of near-burner effects (upstream diffusion of heat and mass around the burner rim), is valid and can be used with confidence.

At p = 1 atm, the mean air and fuel inlet velocities are specified at 30 cm/s and 6.5 cm/s, respectively. The mass flow rates of the air and fuel streams are kept constant as the ambient pressure is varied, i.e., the mean inlet velocities are varied as inversely proportional to pressure.

Table 1 Five sets of pressure and gravity considered.

Set	p (atm)	g (cm/s^2)	g/g_0
1	2	122.5	0.125
2	1.5	217.56	0.222
3	1	490	0.5
4	0.7071	980	1
5	0.5	1960	2

The structures of the flame under the five sets of pressure and gravitational acceleration are first examined in terms of temperature and axial velocity distributions. Fig. 1 displays the 2D distributions of temperature with the peak temperature in each case indicated in the figure caption. The black lines in these color plots represent the stoichiometric mixture fraction (f_{st} = 0.05496) obtained from solving the transport equation for the mixture fraction [16] (solid) and based on the definition of Bilger et al. [17] (dash-dot). The first impression from this figure is that there is a significant change in the flame structure with the variation in the ambient pressure, even though p^2g and the mass flow rates are kept constant. The peak temperature occurs in the annular region low in the flame. The maximum peak temperature is achieved at p = 1 atm and the peak temperature starts to drop slightly as the pressure is either increased or decreased from 1 atm, with slightly more reduction as the pressure is lowered. With decreasing the pressure, however, the temperatures in the centerline region continue to increase. As shown later, this is associated with reduced radiation heat loss from soot as much less soot is formed with decreasing pressure.

Compared to the flame height defined by the location of the stoichiometric mixture fraction on the centerline at p = 1 atm, Fig. 1(c), the flame height (location where the solid black line intersects with the flame centerline) remains almost constant as the pressure is decreased. However, the flame height increases slightly as the pressure is elevated, Figs. 1(a) and 1(b). This is perhaps related to the substantial decrease in the flame temperature in the centerline region, which lowers the overall reaction process more than the enhancement by the increased mixture density (through elevated pressure). On the other hand, the flame height defined by the stoichiometric mixture fraction due to Bilger et al. [17] (black dash-dot line) is increasingly shorter than that from solving the mixture fraction transport equation as the pressure is decreased. Note that the flame height defined by the mixture fraction due to Bilger et al. [17] agrees well with that defined by the axial location where the centerline temperature peaks. Therefore, the mixture fraction defined by Bilger et al. [17] is preferred to locate the flame front in diffusion flames.

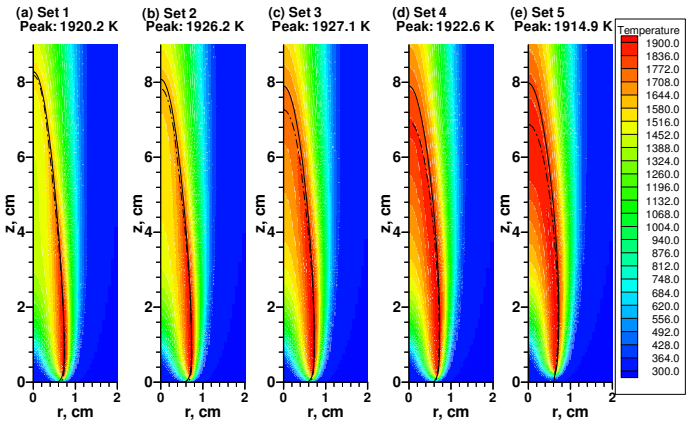

Fig. 1 Temperature distributions with the stoichiometric mixture fraction plotted as black lines.

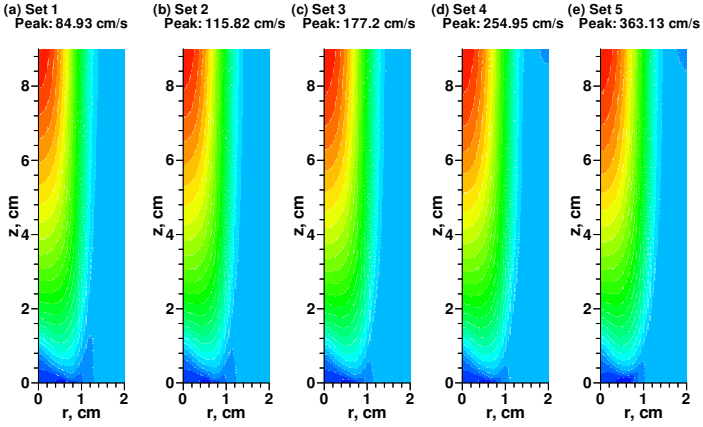

Fig. 2 Axial velocity distributions.

Figure 2 displays the axial velocity distributions. Due to large differences in the axial velocity among the five sets of pressure and gravitational acceleration, each plot uses a different color scale from 0 to its own maximum value indicated in the figure caption. These color contours were

generated using 26 uniform levels between 0 and their respective peak axial velocities. The peak axial velocity (at z = 9 cm on the flame centerline) varies significantly from 84.93 cm/s at p = 2 atm, Fig. 2(a), to 363.13 cm/s at p = 0.5 atm, Fig. 2(e). These results are expected under conditions of fixed mass flow rates and p^2g. With increasing the pressure, both the inlet velocities of the air and fuel streams and the gravitational acceleration decrease. Both factors contribute to the lowered axial velocity shown in Fig. 2, especially the reduced gravitational acceleration.

Such a factor of four variation in the axial velocity suggests that the residence time of a fluid parcel from the burner exit surface to a given height in the flame could be very different. To quantitatively illustrate this point, Fig. 3 compares the residence times for a fluid parcel along the flame centerline. As anticipated from the approximately factor of four increase in the axial velocity as the pressure is decreased from 2 atm to 0.5 atm, the corresponding residence time decreases by about a factor of four. This substantial variation in the residence time from one set of pressure/gravitational acceleration to another implies that certain aspects of the laminar diffusion flame that are kinetically controlled could be quite different, such as soot formation, rendering the p^2g scaling relationship no longer useful for investigating soot formation at reduced buoyancy by conducting experiments at lower pressures.

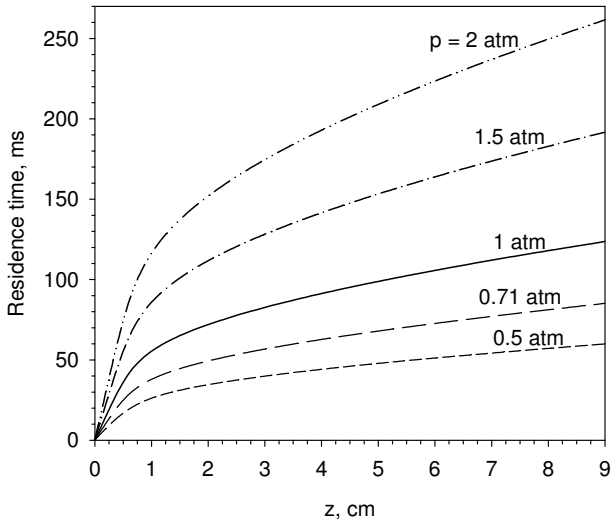

Fig. 3 Variations of residence time of a fluid parcel along the flame centerline.

Distributions of soot volume fraction for the five sets of pressure/gravitational acceleration are compared in Fig. 4. Note that these color contours are generated using 26 uniform color scales from 0 to their respective peak soot volume fractions due to the large variation from one case to another. Several observations can be made from this figure. First, the visible flame height due to soot luminosity increases quite significantly with increasing pressure from about 62 mm at p = 0.5 atm, Fig. 4(e), to about 80 mm at p = 2 atm, Fig. 4(a). Secondly, the peak soot volume fraction also increases very rapidly as the pressure is increased, from 0.11 ppm at p = 0.5 atm to 3.79 ppm at p = 2 atm. Thirdly, the relative concentration of soot in the flame centerline region decreases with increasing pressure. It is well known from laminar diffusion flame experiments conducted at elevated pressures and earth gravity that more soot is produced as the pressure is increased [23-25]. The main mechanism for the effect of pressure on soot formation was found to be through its direct influence on the density mixture, which in turn alters the reaction rates of both gas-phase and soot chemistry. It has also been made clear that reduced buoyancy in general also enhances soot formation [26,27]. Therefore, under conditions of constant p^2g and constant mass flow rates of fuel and air stream it is expected that more soot is formed as the pressure is increased, since both elevated pressure and reduced buoyancy prompt soot formation.

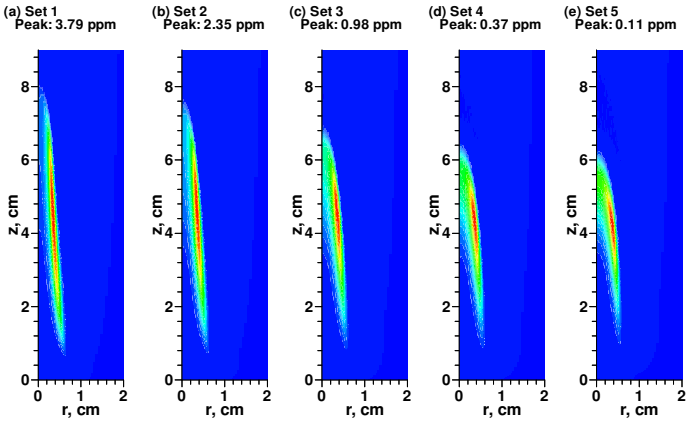

Fig. 4 Distributions of soot volume fraction.

To gain insights into why there are such significant variations in the soot volume fraction with varying pressure, the distributions of acetylene mass fraction, soot nucleation rate, and soot surface growth rate are plotted in Figs. 5-7, respectively. The mass fraction of C_2H_2 increases somewhat significantly with decreasing the pressure, Fig. 5. Due to the coupling between gas-phase chemistry and soot chemistry, the lower C_2H_2 mass fraction at higher pressure is primarily attributed to the conversion of C_2H_2 to soot, while the gas-phase chemistry also plays a role through temperature and enhanced reaction rates. Although soot nucleation rates are much lower than soot surface growth rates, nucleation is the bottle-neck of the soot formation process. At higher pressures, e.g., Figs. 6(a) and 7(a), strong soot nucleation and surface growth occur in the annular region low in the flame as a result of high temperature and high reactant concentration (through pressure), which rapidly depletes the C_2H_2 concentration. Consequently, the nucleation rates in the centerline region are very low, Fig. 6. This is why soot volume fractions in the centerline region are very low as the pressure is increased, Fig. 4. It should be pointed out that residence time also plays an important role in determining the soot surface growth rates

(through available soot surface area) shown in Fig, 7, besides temperature, acetylene concentration, and nucleation rate.

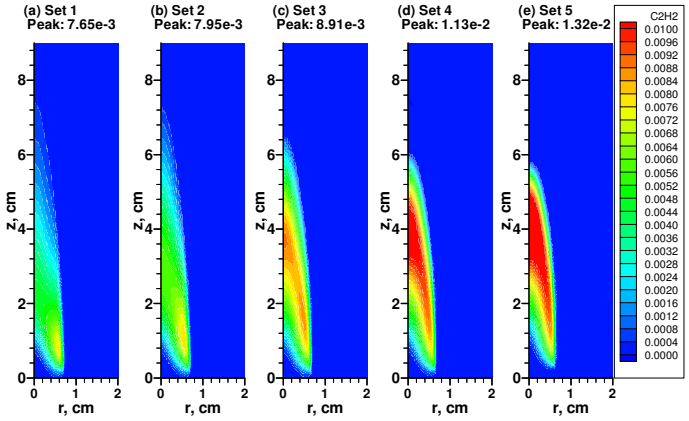

Fig. 5 Distributions of mass fraction of C_2H_2.

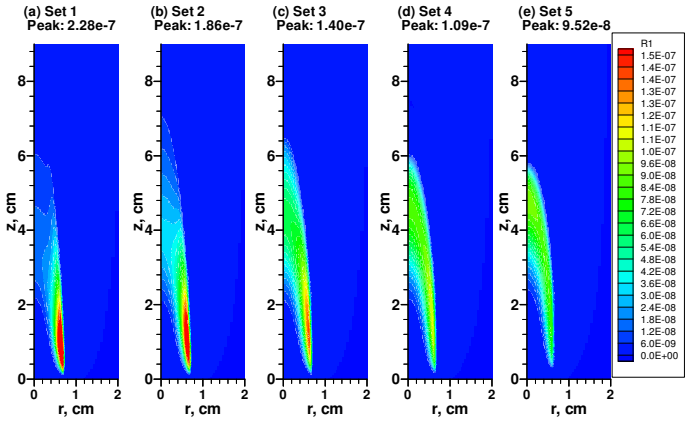

Fig. 6 Distributions of soot nucleation rate (g cm^{-3} s^{-1}).

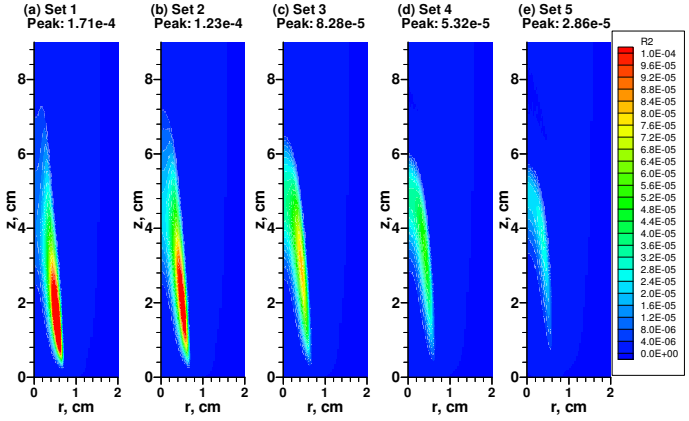

Fig. 7 Distributions of soot surface growth rate (g cm^{-3} s^{-1}).

The results shown in Fig. 4 clearly indicate that soot formation characteristics at lower pressure/higher gravity, Fig. 4(e), are very different from those at higher pressure/lower gravity, Fig. 4(a). For this reason, the p^2g scaling relationship derived by Davis et al [3] should not be used to infer soot formation in reduced gravity by conducting experiments under reduced pressure as advocated by Faeth et al. [1,5]. It is interesting to notice that Davis et al. [3] made the following cautious statement in their study: "Clearly use of this procedure to attain very small effective gravitational accelerations appears unreasonable, as chemical kinetics could certainly not be ignored at the low pressures required. Additionally, enhanced soot production at low g would not be simulated by this pressure variation technique."

As noted in the Introduction, the p^2g scaling relationship was derived based on the flame sheet approximation, unity Lewis numbers, and neglect of thermal radiation transfer by maintaining constant Richardson, Reynolds, and Peclet numbers. The numerical results obtained in this work suggest that there are significant variations in the flame structure and soot formation characteristics for a laminar diffusion flame under conditions of constant mass flow rates of fuel and air streams and p^2g. The reasons for the failure of this scaling relationship for the purpose of soot study include the strong pressure dependence of residence time and reaction rates and the enhanced soot formation and enhanced radiation heat loss, which in turn lowers the flame temperature, as the pressure is increased.

CONCLUSIONS

Detailed numerical calculations were conducted in a laminar coflow CH_4/air diffusion flame with soot formation for five sets of pressure and gravitational acceleration under conditions of constant p^2g and mass flow rates of the fuel and air streams. The numerical results indicate that there are substantial variations in the flame structure, visible flame height, and soot volume fraction as the pressure is varied even though p^2g is fixed. The main reasons for the breakdown of this so-called p^2g scaling relationship are strong variations in residence time, overall chemical reaction rates, and flame temperature as the pressure is varied. Therefore, this scaling relationship should not be used to infer soot formation characteristics in weakly buoyant flames by conducting experiments at reduced pressures.

REFERENCES

1. Mortazavi, S., Sunderland, P. B., Jurng, J., Köylü, Ü. Ö., and Faeth, G. M., 1993, "Structure of Soot-Containing Laminar Jet Diffusion Flames," AIAA 93-0708, 31st Aerospace Sciences Meeting & Exhibit, Reno, NV.
2. Sunderland, P. B., Mortazavi, Faeth, G. M., and Urban, D. L., 1994, "Laminar Smoke Points of Nonbuoyant Jet Diffusion Flames," Combust. Flame, **96**, pp. 97-103.
3. Davis, R. W., Moore, F. E., Santoro, R. J., and Ness, J. R., 1990, "Isolation of Buoyancy Effects in Jet Diffusion Flame Experiments," Combust. Sci. Tech., **73**, pp. 625-635.

4. Faeth, G. M., 1991, "Homogeneous Premixed and Nonpremixed Flames in Microgravity: A Review," Proceedings of the AIAA/IKI Microgravity Science Symposium, AIAA, Washington, pp. 281-293.
5. Köylü, Ü. Ö., Sunderland, P. B., Mortazavi, S., and Faeth, G. M., 1994, "Soot Nucleation and Growth in Waekly-Buoyant Laminar Jet Diffusion Flames," AIAA 94-0428, 32nd Aerospace Sciences Meeting & Exhibit, Reno, NV.
6. Kuo, K. K., 1986, *Principle of Combustion*, Wiley, New York, Chap. 3.
7. Kee, R. J., Grcar, J. F., Smooke, M. D., and Miller, J. A., "A Fortran Program for Modeling Steady Laminar One-Dimensional Premixed Flames," SANDIA Report, SAND85-8240, Reprint, 1994.
8. Leung, K. M., Lindstedt, R. P., and Jones, W. P., 1991, "A Simplified Reaction Mechanism for Soot Formation in Nonpremixed Flames," Combustion and Flame, **87**, pp. 289-305.
9. Liu, F., Guo, H., Smallwood, G. J., and Gülder, Ö. L., 2002, "Effects of Gas and Soot Radiation on Soot Formation in a Coflow Laminar Ethylene Diffusion Flame," Journal of Quantitative Spectroscopy and Radiative Transfer, **73**, pp. 409-421.
10. Nagle, J., and Strickland-Constable, R. F., 1962, "Oxidation of Carbon between 1000-2000°C," Proceedings of the Fifth Conference on Carbon, pp. 154-164.
11. Moss, J. B., Stewart, C. D., and Young, K. J., 1995, "Modeling Soot Formation and Burnout in a High Temperature Laminar Diffusion Flame Burning under Oxygen-Enriched Conditions," Combust. Flame, **101**, pp. 491-500.
12. Bradley, D., Dixon-Lewis, G., Habik, S. El-Din., and Mushi, E. M. J., 1984, "The Oxidation of Graphite Powder in Flame Reaction Zones," Proceedings of the Combustion Institute, **20**, pp. 931-940.
13. Liu, F., Guo, H., and Smallwood, G. J., 2004, "Effects of Radiation Model on the Modeling of a Laminar Coflow Methane/Air Diffusion Flame," Combustion and Flame, **138**, pp. 136-154.
14. Liu, F., and Smallwood, G. J., 2004, "An Efficient Approach for the Implementation of the SNB based Correlated-k Method and Its Evaluation," Journal of Quantitative Spectroscopy and Radiative Transfer, **84**, pp. 465-475.
15. Smith, G. P., Golden, D. M., Frenklach, M., Moriarty, N. W., Eiteneer, B., Goldenberg, M., Bowman, C. T., Hanson, R. K., Song, S., Gardiner Jr., W. C., Lissianski, V. V., and Qin, Z., http://www.me.berkeley.edu/gri_mech/.
16. Pitsch, H., and Peters, N., 1998, "A Consistent Flamelet Formulation for Non-Premixed Combustion Considering Differential Diffusion Effects," Combustion and Flame, **114**, pp. 26-40.
17. Bilger, R. W., Stårner, S. H., and Kee, R. J., 1990, "On reduced mechanisms for methane-air combustion in nonpremixed flames," Combustion and Flame, **80**, pp. 135-149.
18. Patankar, S. V., 1980, *Numerical Heat Transfer and Fluid Flow*, Hemisphere, New York.
19. Liu, Z., Liao, C., Liu, C., and McCormick, S., 1995, "Multigrid Method for Multi-Step Finite Rate Combustion," AIAA 95-0205.
20. Snelling, D. R., Thomson, K. A., Smallwood, and G. J., Gülder, Ö. L., 1999, "Two-Dimensional Imaging of Soot Volume Fraction in Laminar Diffusion Flames," Applied Optics, **38**, pp. 2478-2485.
21. Santoro, R. J., Semerjian, H. G., and Dobbins, R. A., 1983, "Soot Particle Measurements in Diffusion Flames," Combustion and Flame, **51**, pp. 203-218.
22. Smyth, K. C., Miller, J. H., Dorfman, R. C., Mallard, W. G., and Santoro, R. J., 1985, "Soot Inception in a Methane/Air Diffusion Flame as Characterized by Detailed Species Profiles," Combustion and Flame, **62**, pp. 157-181.
23. Liu, F., Thomson, K. A., Guo, H., and Smallwood, G. J., 2006, "Numerical and experimental study of an axisymmetric coflow laminar methane-air diffusion flame at pressures between 5 and 40 atmospheres," Combustion and Flame, **146**, pp. 456-471.
24. Thomson, K. A., Gülder, Ö. L., Weckman, E. J., Fraser, R. A., Smallwood, G. J., and Snelling, D. R., 2005, "Soot concentration and temperature measurements in co-annular, nonpremixed CH_4/air laminar flames at pressures up to 4 MPa," Combustion and Flame, **140**, pp. 222-232.
25. McCrain, L. L., and Roberts, W. L., 2005, "Measurements of the soot volume field in laminar diffusion flames at elevated pressures," Combustion and Flame, **140**, pp. 60-69.
26. Megaridis, C. M., Griffin, D. W., and Konsur, B., 1996, "Soot-field structure in laminar soot-emitting microgravity nonpremixed flames," Proc. Combust. Inst., **26**, pp. 1291-1299.
27. Greenberg, P. S., and Ku, J. C., 1997, "Soot volume fraction maps for normal and reduced gravity laminar acetylene jet diffusion flames," Combust. Flame, **108**, pp. 227-230.

